Escola de Primavera de Transição e Turbulência
Blumenau 2020

ABCM Associação Brasileira de Engenharia e Ciências Mecânicas

12th Spring School on Transition and Turbulence
September 21st-25th, 2020, Blumenau, SC, Brazil

EPTT-2020-0041
ANALYSIS OF THE EFFECTS OF TURBULENCE CLOSURE MODELS ON WALL FILM MODELLING

Francisco José de Souza
Bruno Silva de Lima
João Rodrigo Andrade
Dep. of Mechanical Engineering, Federal University of Uberlândia, Fluid Mechanics Laboratory, Campus Santa Mônica, Uberlândia, MG, Brazil.
francisco.souza@ufu.br, brunosilvadelima@hotmail.com, joao.andrade@ufu.br

Carlos Antônio Ribeiro Duarte
Dep. of Engineering, Federal University of Goias, Av. Dr. Lamartine Pinto de Avelar, 1120, Catalao, Goias, Brazil.
carlosduarte@ufg.br

Martin Sommerfeld
Institut für Verfahrenstechnik (IVT) OVGU - Die Otto-von-Guericke-Universität Magdeburg, Universitätsplatz 2, 39106 Magdeburg, Germany
martin.sommerfeld@ovgu.de

Abstract. *Liquid film formation is a phenomenon widely found in industrial processes. Intended or not, it can be found in process such as coating, painting, steam power generation, refrigeration systems, and fuel injection. This paper presents an study of simulations by means of Eulerian-Lagrange approach of thin liquid formation in a liquid jet in cross-flow using Euler Wall Film (EWF) modelling. The EWF model is derived from classical fluids mechanics theory and accounts for mass and momentum conservation. This model uses a two dimensional form of mass and momentum conservation for the liquid phase in a three dimensional mesh. The main purpose of this work is to verify the effects of turbulence closure models on the on the thin liquid film modelling. To verify the employed model, the numerical results are compared with a cross flow physical experimentation developed by Shedd et al (2009). The current implementation was carried out using an in-house code called Unscyfl3D, This code was validate against results for a wide range of multi-phase flow physical experiments. The main results showed that the breakup model proved to be sensitive against the turbulence closure model. This fact directly affects the liquid film formation while the droplets distribution inside the domain affects the splashing probability, which is a fundamental step on the EWF model.*

Keywords: *Thin liquid film formation, Liquid jet in cross flow, Eulerian Wall Film (EWF)*

1. INTRODUCTION

The study of multiphase flows is of great importance since there is a wide range of phenomena described by the interaction between fluids. Among them there are natural processes such as the rain drop, which can cause soil erosion and is also a medium to transport bacteria and spores.The impact of rain drops also influences in the air-sea gas exchange as well as in the damping of wave motion Morton *et al.* (2000). There are also industrial processes involving multiphase flows such as coating, painting, fuel injection and irrigation. To effective achieve the desired results in each of these processes, the instruments must be correctly characterized and applied. For instance, the injection of fuel in an internal combustion engine is subjected to wall impingement, which directly affects the outcome of the combustion process. The improvement in the characteristics of this process makes the processes more efficient and less environmentally degrading. Baumgarten (2006), Shim *et al.* (2008), Heywood (1988).

The correct usage of irrigation instruments leads to a decrease of water consumption as well as avoid soil erosion. Noticing that sprinkler irrigation is responsible for half of annual consumption of water, the optimization of this process is extremely important. Stevenin *et al.* (2016).

Thin liquid films are often found in engineering applications with thicknesses ranging from micrometer scales to millimeter scales. Thin liquid film flow modeling and characterization is important for many applications, including steam power generation, crude oil supply and refining, chemical processing and refrigeration systems. Many methods for measuring and predicting these phenomena have being developed including physical experiments as well as numerical-

computational techniques. The improvement in the characteristics of this process makes the processes more efficient and less environmentally degrading. Shedd and Newell (1997) For that purpose, numerical methods have been increasingly used in complex engineering problems, providing results in scenarios where experiments may not be feasible, reducing costs and development time. Fontes *et al.* (2018a)

In this paper, the evaluation of the effects of turbulence closure modelling on the liquid film formation using Euler Wall Film modelling is presented. For that three different Reynolds Averaged Navier-Stokes (RANS) turbulence closure models were tested: k-ϵ , optmized k-ϵ and Shear Stress Transport (SST). The basic difference for the k-ϵ and optmized k-ϵ are the constant values for turbulence closure model. In the second case, the values of the constants of the model (C_μ, $C_{\epsilon 2}$, $C_{\epsilon 1}$) were optimized for jet-in-crossflow (JIC) simulations by Ray *et al.* (2014), where more details can be found. The choice of turbulence closure models is based upon the studied carried out by Duarte *et al.* (2020), in which an extensively comparison between the models was carried out. An analysis of the droplet distribution and film thickness at the bottom wall of the computational domain is then presented.

To carry out the simulations the in-house code Unscyfl3D was used. This code is characterized by simulating laminar and turbulent multiphase flows. For that, the Navier-Stokes Equations are solved in an incompressible form through the method of finite volumes in unstructured meshes and colocalized arrangement. For the pressure-velocity coupling the SIMPLE algorithm was implemented. This code has already been widely validated with relevant results in the literature.

2. MODEL DESCRIPTION

For the continuous phase the basic equations for fluid flow are mainly conservation of mass and momentum. Several authors also add the equation of energy conservation, but this equation is not considered in this work. Equation 1 represents the conservation equation of mass in its three-dimensional form for incompressible flows. The equation of momentum conservation is represented in Equation 2. Versteeg and Malalasekera (2007)

$$\frac{\partial \bar{u}_i}{\partial x_i} = 0, \tag{1}$$

$$\frac{\partial(\rho \bar{u}_i)}{\partial t} + \frac{\partial(\rho \bar{u}_i \bar{u}_j)}{\partial x_j} = -\frac{\partial p}{\partial x_i} + \frac{\partial}{\partial x_j}\left[(\mu + \mu_t)\left(\frac{\partial \bar{u}_i}{\partial x_j} + \frac{\partial \bar{u}_j}{\partial x_i}\right)\right] + \rho g_i + s_{u_i}, \tag{2}$$

in which, x is the position, g_i are the gravity vector components, t is the time and $\bar{u}$ is the velocity in i and j directions, s_{u_i} is the source terms in the x, y and z directions, μ is the fluid dynamic viscosity, ρ is the fluid density, μ_t is the eddy viscosity, and τ stands for tension.

Small droplets follow a Lagrangian methodology, being represented as discrete phase. To calculate their velocity and position, the equations of motion are used, represented by Equation 3 and Equation 4 respectively. Fontes *et al.* (2018b)

$$m_p \frac{du_{pi}}{dt} = F_d + F_{w,b}, \tag{3}$$

$$\frac{dx_{pi}}{dt} = u_{pi}, \tag{4}$$

in which the subscript p indicates that it is related to a particle or droplet, x is the position and m is the mass.

As represented in Equation 3 only two forces are considered. The drag force F_d, represented in Equation 5 and the combined buoyancy-weight force $F_{w,b}$ represented in Equation 6. Fontes *et al.* (2018b)

$$F_d = m_p \frac{3\rho C_D}{4\rho_p d_p}(u_{i,t} - u_{pi}), \tag{5}$$

$$F_{w,b} = (1 - \frac{\rho}{\rho_p}) m_p g_i, \tag{6}$$

in which $u_{i,t}$ is the instantaneous fluid velocity, calculated as the mean velocity plus a fluctuating component ($u_{i,t} = u_i + u_i^{'}$), calculated as the Langevin dispersion model proposed by Sommerfeld (2001). In this model, C_d is the drag coefficient and it is calculated according to Equation 7, which represents empirical correlations considering rigid spherical droplets. Fontes *et al.* (2018b)

$$C_d = \begin{cases} \frac{24}{Re_p}(1 + 0.15 Re_p^{0.687}) : Re_p < 1000 \\ 0.424 : Re_p > 1000 \end{cases}, \tag{7}$$

in which Re is the Reynolds number.

The EWF model was developed to simulate the behaviour of thin liquid film formation and propagation after droplet collection. Using the consideration of thin film, lubrication theory was used to develop this model. According to Ingle *et al.* (2014) the process of film formation can be described in five phenomena. The first is particle collection and film formation, in which droplets collide on the wall surface and may form liquid film. The second is film transport, in which the formed film moves due to shear forces between the film and the Eulerian phase. The third is the splashing of new droplets on the liquid film surface, in which the impinging droplets instead of forming film liquid can remove liquid from the liquid film. The fourth is the striping, in which droplets can separate from the film liquid due to shear forces between the liquid film and the Eulerian phase. The fifth is the separation, in which the liquid reaches a geometry degree, sometimes the end of a filmer wall, may arising new droplets and ligaments.

For the EWF model the overall system mass must be conserved. In the case of the EWF this conservation of mass is carried out in a two dimensional model in a three dimensional domain. For that a transient explicit formulation is used, as represented in Equation 8. Ingle *et al.* (2014)

$$\left(\frac{\partial h}{\partial t}\right) + \nabla_s \cdot \left[h\vec{V_l}\right] = \left(\frac{\dot{m}_s}{\rho_l}\right), \tag{8}$$

in which $\vec{V_l}$ is the mean film velocity, h is the film height, ∇_s is the surface gradient operator, ρ_l is the liquid density and $\dot{m}_s$ is the mass source term per unit wall area due to the phenomena described before.

The overall momentum conservation is represented by Equation 9. The first term on the left hand side of Equation 9 represents the transient effect. The second term represents the convection effects. On the right hand side the first term represents three effects, the gas-flow pressure, the normal gravity component and surface tension. The second term represents the effect of gravity parallel to the surface. The third term is the viscous shear force at the interface between the Eulerian phase and the liquid film. The fourth term represents the viscous force in the liquid film. The fifth term is the source term. Ingle *et al.* (2014)

$$\left(\frac{\partial h\vec{V_l}}{\partial t}\right) + \nabla_s \cdot \left[h\vec{V_l}\vec{V_l}\right] = -\left(\frac{h\nabla_s P_L}{\rho_l}\right) + \left(\vec{g}_\tau\right)h + \frac{3}{2\rho_l}\vec{\tau}_{fs} - \frac{3\nu_l}{h}\vec{V_l} + \frac{\dot{q}}{\rho_l}, \tag{9}$$

in which

$$P_L = P_{gas} + P_h + P_\sigma, \tag{10}$$

$$P_h = -\rho h\left(\vec{n}\cdot\vec{g}\right), \tag{11}$$

$$P_\sigma = \sigma\nabla_s \cdot \left(\nabla_s h\right), \tag{12}$$

The source terms account for the modelling of the interaction between the EWF model with the Lagrangian phase. For that the above mentioned particle collection, splashing, stripping and separation phenomena are modeled through sub models for source terms.

Discrete particles (Lagrangian phase) after impinging on the wall can be absorbed by the liquid film. The mass of the discrete phase is then added to the liquid film as represented by Equation 13 and its momentum as represented by Equation 14. Ingle *et al.* (2014)

$$\dot{m}_s = \dot{m}_p, \tag{13}$$

$$\vec{q}_s = \dot{m}_p \cdot \left(\vec{V}_P - \vec{V_l}\right), \tag{14}$$

in which $\dot{m}_p$ is the flow rate of the droplet impinging on the wall surface, $\vec{V}_P$ is the particle velocity and $\vec{V_l}$ is the liquid film velocity.

The outcomes of a droplet impingement are based on criteria regarding the liquid properties, the properties of the impact surface and also the surrounding fluid. The surface of impact can be solid or liquid. In the case of impacting in a liquid film, according to the EWF approximations, the liquid covering a solid surface must be thin.

In order to model the collision outcomes of the droplets the correlations presented by Kuhnke (2004) were used. These correlations were based in two non dimensional numbers represented in Equation 15 and Equation 16.

$$T^* = \frac{T_w}{T_{sat}}, \tag{15}$$

$$K = \frac{(\rho D)_d^(3/4)(u)_d^(5/4)}{(\sigma)_d^(1/2)(\mu)_d^(1/4)}, \tag{16}$$

There are four possible outcomes according to this methodology: rebound, splash, absorption or thermal breakup. To summarize these outcomes according to the presented non dimensional numbers Kuhnke (2004) constructed a regime map as represented in Figure 1. For the current studied case the wall temperature is below the droplet temperature, implying that only absorption and splash are possible.

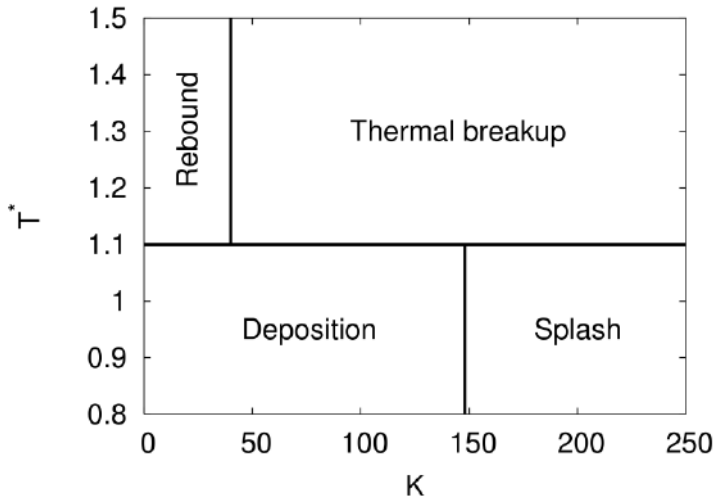

Figure 1: Regime map for spray/wall-interaction according to (Kuhnke, 2004)

The conditions at the phase interface are approximated as a film roughness approach. For that, the film roughness is calculated as in Equation 17. This equation was adapted from Stanton and Rutland (1998) bearing in mind that in his case the evaporation was considered and in the current work the equation of energy is not solved.

$$k_s = 2\Phi\delta, \tag{17}$$

in which k_s is the film roughness and Φ can be estimated as in Equation 18.

$$\Phi = 0.735 + 0.009255\bar{\tau}, \tag{18}$$

in which $\bar{\tau}$ is the average shear stress.

The influence of the liquid film roughness on the air flow can be estimated using the logarithmic law of the wall as in Equation 19.

$$u^+ = \frac{1}{\kappa} ln(y^+) + C, \tag{19}$$

in which the constant C is a function of Reynolds number, defined as in Equation 20.

$$Re_{k_s} = \frac{k_s u_\tau}{\nu}, \tag{20}$$

And C can then be estimated as in Equation 21.

$$C = \begin{cases} 5.15 : Re_{k_s} < 5 \\ 1.5497 + 19.1log(Re_{k_s}) - 14.43[log(Re_{k_s})]^2 + 3.31[log(Re_{k_s})]^3 \\ -\frac{1}{\kappa}ln(Re_{k_s}) : 5 \leq Re_{k_s} \leq 70 \\ 8.5 - \frac{1}{\kappa}ln(Re_{k_s}) : 70 < Re_{k_s} \end{cases}, \tag{21}$$

3. CASE DESCRIPTION

The experiment consists of a jet that interacts with a cross flow. Figure 2 represents the liquid jet dynamics in the system, which is very similar to the injection of fuel in air-blast atomizers. After liquid injection, it interacts with a cross flow of air. The air stream causes this liquid to undergo a first breakup process as well as bends the liquid jet in the flow direction. The jet and the formed droplets may collide with the wall forming a thin liquid film on the surface. This liquid film flows in the direction of the airflow until it goes out of the plate and interacts with the secondary airstream undergoing a film breaking process.

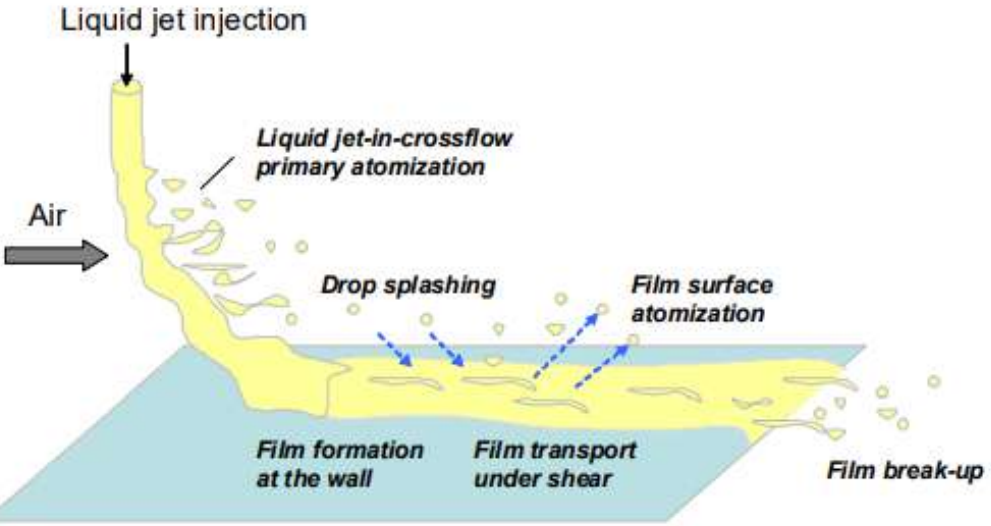

Figure 2: Physics of the jet and film formation. (Shedd *et al.*, 2009)

The test bench is illustrated on Figure 3. The test section and the vessel are made of polycarbonate, which facilitate optical access. There are two air entrances, a larger one where the air flows velocity is represented by U_1 called main way and a smaller with velocity of U_2. The light blue region represented in Figure 3 is the liquid issuing out from the nozzle, interacting with the main air flow, impinging on the surface, forming a thin film liquid and finally interacting with the secondary flow. Shedd *et al.* (2009)

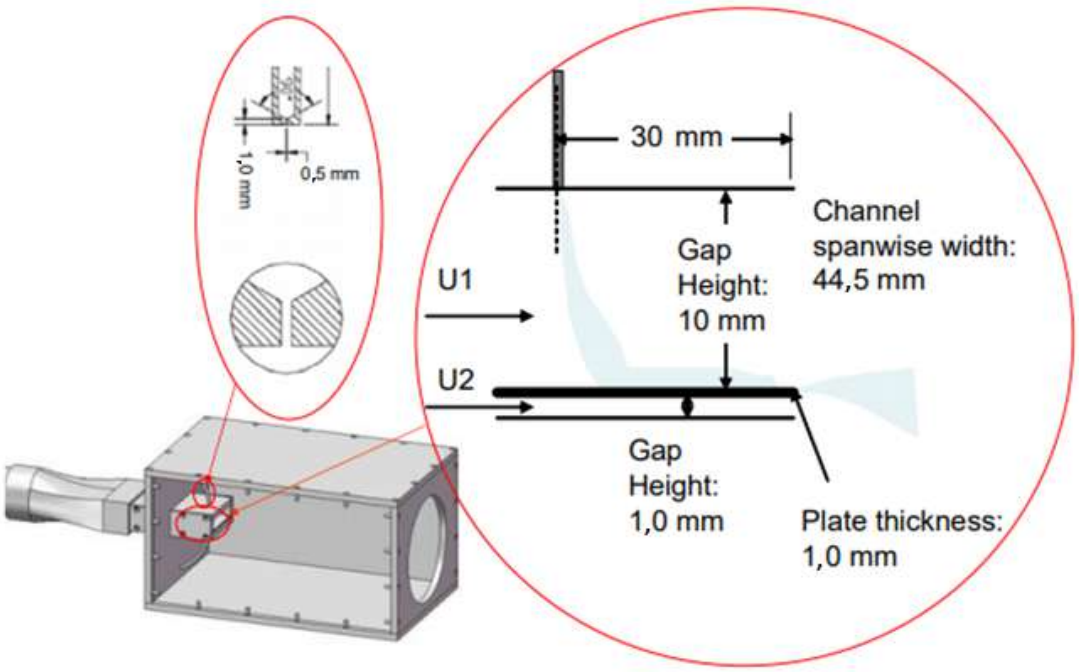

Figure 3: Experimental setup. (Shedd *et al.*, 2009)

4. COMPUTATIONAL DOMAIN AND MESH PARAMETERS

The computational domain for the test case is represented in Figure 4a with its main dimensions. The nozzle is represented by the blue cylinder, which is $6.34\ mm$ away from the inlet. The nozzle hole diameter is $0.5\ mm$. The coordinate system center is represented by the dot at the center of the nozzle. For the simulations in this paper only the main air inlet was considered, bearing in mind that it does not affect the liquid film formation on the wall. The mesh for this computational domain is illustrated on Figure 4b. The mesh has a total number of nodes of 662240 and 637767 elements. The mesh generation was made using ICEM-ANSYS software. Near wall regions were refined to capture the physics of the near wall effects. Using empirical data, a value of $y^+ = 1$ was chosen to be used. More details can be found in White (1962). Regions near the injector (in the center of the mesh) are also more refined. For these simulations the injection of droplets follows a Lagrangian methodology. As only Lagrangian droplets are considered, the geometry part of the nozzle entrance was geometrically unconsidered.

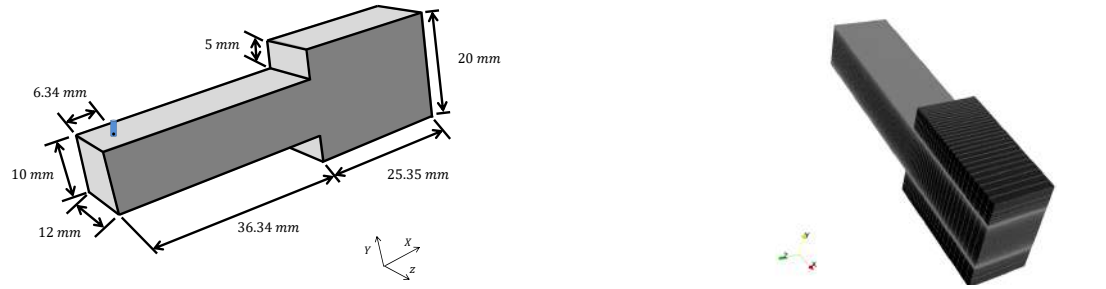

(a) Computational domain dimensions. (b) Euler-Lagrangian full domain mesh.

Figure 4: Computational domain and mesh

5. BOUNDARY AND INITIAL CONDITIONS

The boundary conditions for the studied case are represented in Figure 5.

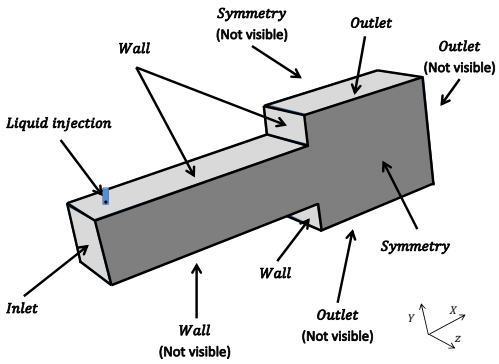

Figure 5: Boundary conditions.

For the inlet boundary condition air is injected at 81 m/s. In the inlet boundary condition the condition of escape is considered for the droplets.

For the outlet boundary condition an absolute pressure of 0 Pa was considered. In the outlet boundary conditions the condition of escape is considered for the droplets.

For the symmetry boundary condition symmetry was considered. In the symmetry boundary condition the condition of escape is considered for the droplets.

For the wall boundary condition no slip conditions were considered. For the bottom wall, wall film formation was considered. For the top walls only reflection was taken in account for the droplets.

In the currently implementation parcels containing droplets with the same radius and velocity are injected as liquid phase. Two cases were tested. The difference between them is only the velocity of liquid injection and the liquid mass flow. The first case considered an injection of mineral spirits with 12.7 m/s (case 1) and the second case with 17 m/s (case 2). For the Lagrangian droplets an initial radius of 0.5 mm was considered, which is the nozzle diameter.

For initial conditions only air was considered inside the domain. The velocity was set to zero.

6. CASE SETUP

The convergence criterion for each iteration was set to 10^{-4} while the divergence criterion was set to 10^{11}. The numerical advective scheme used is the second-order upwind. The maximum number of SIMPLE iterations per time step is set to 20. The two-way coupling methodology was set for the coupling of fluid flow and particles motion. This means that the source terms momentum due to the droplets will be added to the conservation equations for the Eulerian fluid flow. In this case, the time step for the particles and the fluid must be the same. The number of parcels generated after secondary break up was set to 10.

For the cross flow case the first simulation is in permanent regime and the droplets are not injected. For that 2000 time steps were run, getting absolute residual source sums in the order of 10^{-3}. The resulting flow field is used as initial conditions on the transient simulation.

For the transient simulation 6000 time steps were run with a time step of $2 \cdot 10^{-6}$. After that, the Eulerian flow field is frozen, then the simulation runs just with the droplets. The frozen simulation run for 30000 time steps to get good results for the main average values.

The software is based on the analysis of incompressible flows using finite volume method in unstructured meshes. To couple velocity and pressure the SIMPLE algorithm is used. To store the variable a collocalized arrangement is used. The numerical scheme for diffusive terms is the second order centered differences and for the advective terms the second order upwind. The secondary break up model for the Lagrangian droplets is the ABTAB.

The air is considered to have density, $\rho_g = 1.427\ kg/m^3$, dynamic viscosity, $\mu_g = 1.7894 \cdot 10^{-5}\ kg/m \cdot s$ at 300 K, Richards *et al.* (2016).
The liquid is Mineral Spirits, which has density $\rho_l = 780\ kg/m^3$, dynamic viscosity, $\mu_l = 8.5 \cdot 10^{-4}\ kg/m \cdot s$ and surface tension, $\sigma = 0.024\ N/m$, at 300 K. Shedd *et al.* (2009)

7. RESULTS

This chapter consists in the analysis of liquid film formation using EWF modelling. The validation of the main results was carried out by means of a comparison of the simulation results and data found in the literature. The main findings are here highlighted and discussed.

For the simulations an Intel®Core^{TM} i7-9700 CPU 3.00 GHz with 16 GiB system memory and eight physical cores was used.

The results for the height of the liquid film for the cross flow case were obtained along the white arrow as represented

in Figure 6. The beginning of the white arrow represents x coordinate zero, the same x coordinate position of the injector.

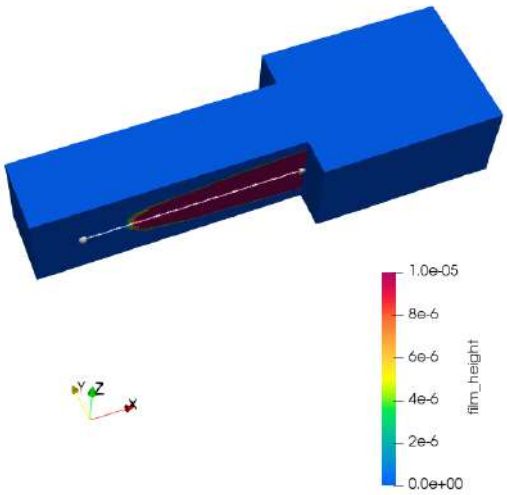

Figure 6: Data acquirement for analysis in the case liquid film formation in cross flow.

The results for film height while using different turbulence closure models are represented in Figure 7 for case 1 and are also compared to experimental data. For this case the time of operation was 5691.989 s for k-ϵ, 9220.531 s for optimized k-ϵ, and 25686.33 s for SST, considering the simulation time of the frozen field with Lagrangian droplets. The number of particles inside the domain was 20809 for k-ϵ, 22435 for optimized k-ϵ, and 134255 for SST. Comparing the models it is possible to observe that there are more secondary droplets for the SST model and also a longer time of operation.

It can be observed from the results that the film liquid height grows progressively until it gets close to the edge. The main observations are that the SST model can better predict the liquid film behaviour as the k-ϵ and the optimized k-ϵ under-predict the liquid film formation. The differences for the k-ϵ and the optimized k-ϵ are mostly that the liquid film formation starts further from the x coordinate of the jet for optimized k-ϵ. Near the end corner there is another difference, where the results for optimized k-ϵ presented smaller values for the liquid film and even a drop on the film height.

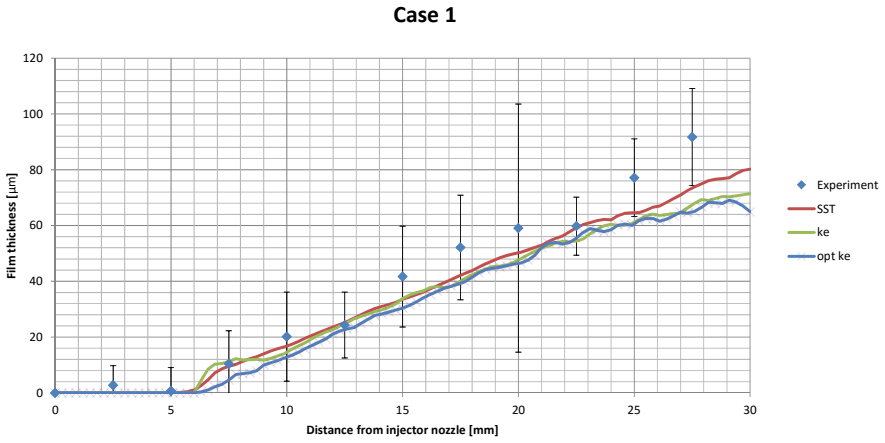

Figure 7: Results of averaged liquid film height for case 1.

For case 1, images of the film liquid on the wall surface are illustrated in Figure 8a for the k-ϵ, in Figure 8b for the optimized k-ϵ, and in Figure 8c for the SST model. The scale is represented differently in these figures when compared to Figure 6 for better visualization of the liquid film height. On this images it observed that the k-ϵ and the optimized k-ϵ behave similar. For the SST case the film liquid height presented a different pattern. In this case, higher liquid films are found on the center of the wall film, while the other two cases presented higher liquid film away from the center line.

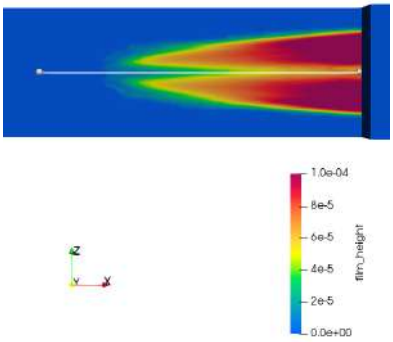

(a) Results of averaged liquid film height for case 1 using k-ϵ turbulence closure model.

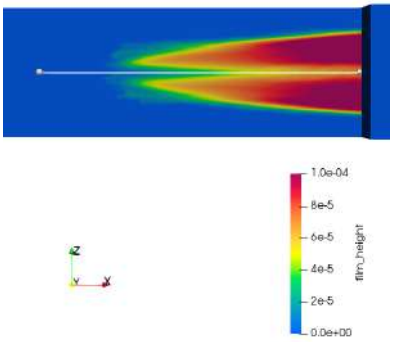

(b) Results of averaged liquid film height for case 1 using optimized k-ϵ turbulence closure model.

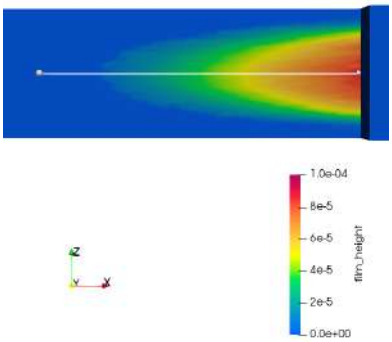

(c) Results of averaged liquid film height for case 1 using SST turbulence closure model.

Figure 8: Liquid film thickness for different turbulence closure models (case 1)

The main differences observed can be partly explained by the droplets behaviour in each case. The droplets are represented for the different models, being Figure 9a for the k-ϵ, Figure 9b for optimized k-ϵ, and Figure 9c for SST. Velocity is plotted for the Eulerian phase. It is observed that for the k-ϵ and optimized k-ϵ that the spray behaviour are similar. The results for the SST turbulence closure model presented more droplets at vertical positions along the domain.

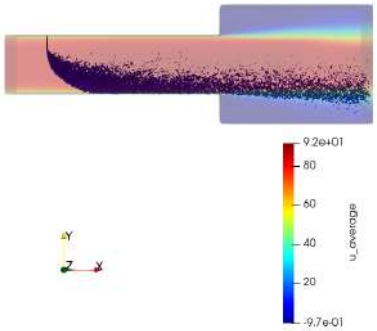

(a) Results of droplets distribution inside the domain for case 1 using k-ϵ turbulence closure model.

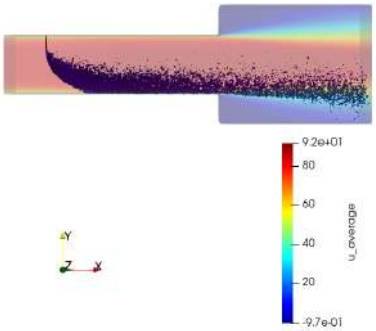

(b) Results of droplets distribution inside the domain for case 1 using optimized k-ϵ turbulence closure model.

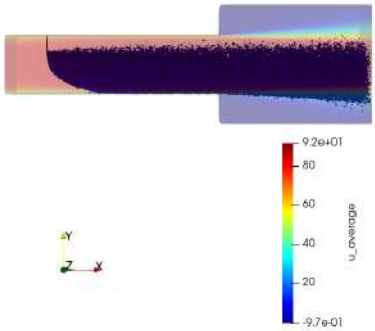

(c) Results of droplets distribution inside the domain for case 1 using SST turbulence closure model.

Figure 9: Results of droplets distribution for different turbulence closure models (case 1)

The droplets are illustrated in Figure 10 for a view of the bottom wall. The droplets prior to the impact on the wall are bigger for k-ϵ models than for SST turbulence closure model. It is also noted an absence of droplets along the center line of the computational domain for the k-ϵ results. This behaviour is due to the interaction of the droplets with the air stream, which presented differences for the different models. The droplets and the film liquid are illustrated in Figure 10b for the optimized k-ϵ turbulence closure model. According to this, it becomes clear that the droplets behaviour formed the film liquid shape represented on Figure 8b. The droplets are represented in Figure 10c for the SST turbulence closure model. It becomes clear from this figure the more evenly distributed concentration of droplets. This distribution generates a liquid film formation with a higher concentration along the center line of the computational as represented on Figure 8c. This behaviour is different from the other models tested. The droplets and the film liquid are represented in Figure 10d to illustrate the droplet distribution on the liquid film formation.

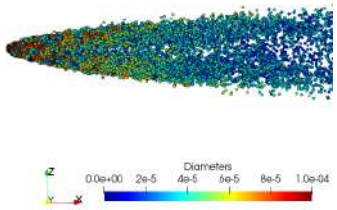

(a) Results of droplets distribution inside the domain for case 1 using optimized k-ϵ turbulence closure model. (Bottom view)

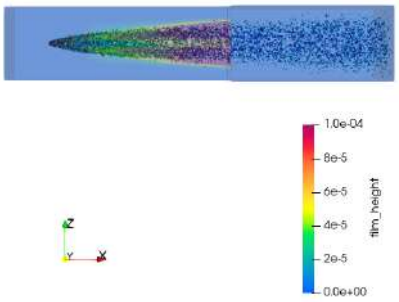

(b) Results of droplets distribution and liquid film height inside the domain for case 1 using optimized k-ϵ turbulence closure model.

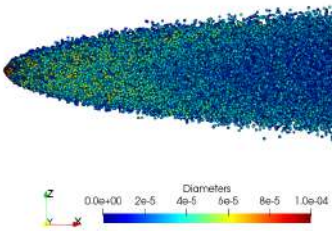

(c) Results of droplets distribution inside the domain for case 1 using SST turbulence closure model. (Bottom view)

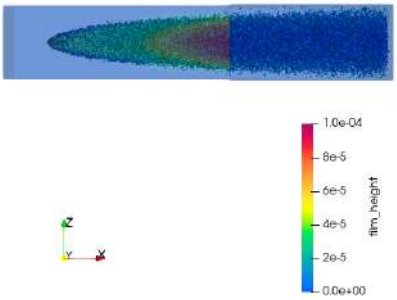

(d) Results of droplets distribution and liquid film height inside the domain for case 1 using SST turbulence closure model.

Figure 10: Results of droplets distribution and liquid film height inside the domain for different turbulence closure models (case 1)

The results of different turbulence closure models are represented in Figure 11 for case 2. It is observed that the liquid film formation for case 2 is bigger than for case 1. The results of film height were obtained along the white line illustrated in Figure 6. For this case the time of operation was 7380.009 s for k-ϵ, 7316.281 s for optimized k-ϵ, and 23702.26 s for SST. The number of particles inside the domain was 6898 for k-ϵ, 7055 for optimized k-ϵ, and 121955 for SST, considering the simulation time of the frozen field with droplets. Again, there is more secondary droplets for the SST case and also a longer time of operation. The main observations are that the SST model can better predict the liquid film behaviour as the k-ϵ and the optimized k-ϵ underpredict the liquid film formation. The differences for the k-ϵ and the optimized k-ϵ in these cases are greater, the liquid film formation starts further from the injection x coordinate in the k-ϵ results and it also presented smaller results. The behaviour of the simulations after 20 mm started to deviate from the physical experiments. An important observation is that the physical experimental data presented a dip in the film height just prior to the edge. This behaviour was not predicted by any of the tested models. It is also observed that the deviations from the experimental results were greater for case 2 when compared to case 1.

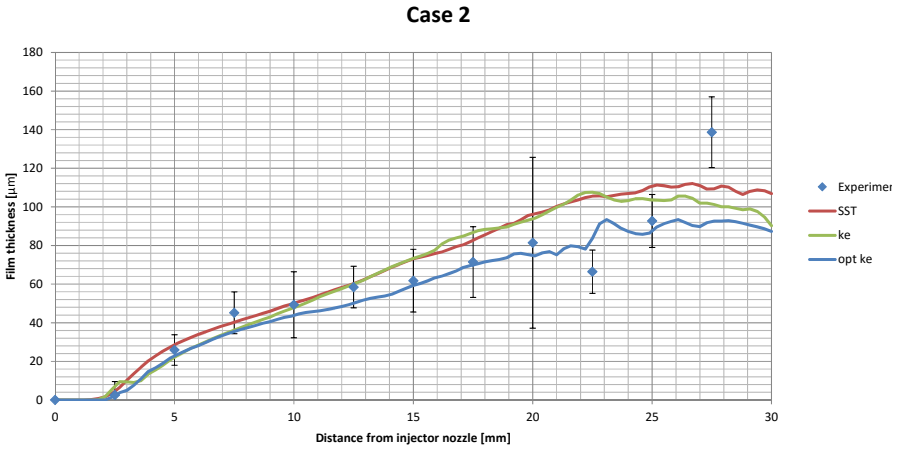

Figure 11: Results of averaged liquid film height for case 2.

For case 2, images of the film liquid are illustrated in Figure 12a for the k-ϵ, in Figure 12b for the optimized k-ϵ, and in Figure 12c for the SST model. On this images it is observed that the k-ϵ and the optimized k-ϵ film shapes are very close to each other, as also observed in case 1. A similar behaviour was found for the SST case when compared to case 1. The film liquid height presented a different pattern from the other two models, with higher liquid films at the center of the wall film. The other two tested models presented higher liquid films away from the center line. As observed in case 1, the main differences observed for case 2 can be partly explained by the droplets behaviour in each case.

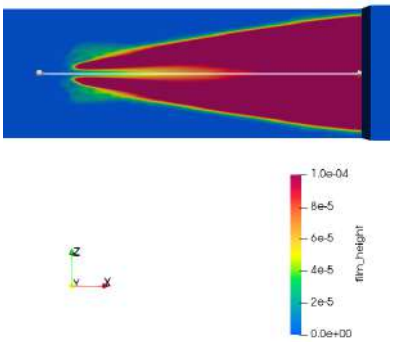

(a) Results of averaged liquid film formed for case 2 using k-ϵ turbulence closure model.

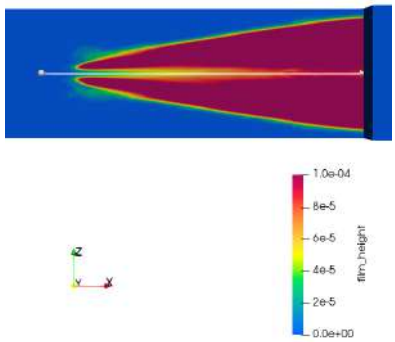

(b) Results of averaged liquid film formed for case 2 using optimized k-ϵ turbulence closure model.

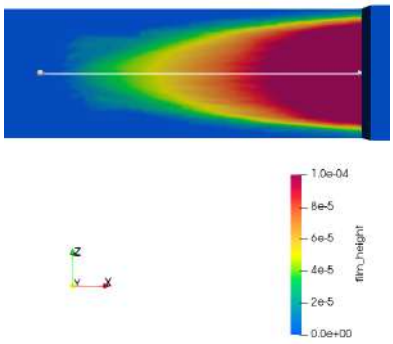

(c) Results of averaged liquid film formed for case 2 using SST turbulence closure model.

Figure 12: Results of droplets distribution for different turbulence closure models (case 2)

8. FINAL REMARKS

The Euler Wall Film approach proved to be an accurate and cheap tool to simulate wall film formation. This methodology was able to capture most of the liquid film formation dynamics and presented good agreement with experimental data, proving to be a powerful tool on the simulation and improvement of industrial process.

Besides that, some phenomena are not completed understood and not all the physics can be captured by this approach, as the dip on case 2. Therefore, the hybrid approach is believed to further the knowledge in this field. For that, future works will involve experiments with the hybrid Euler/Lagrangian approach.

9. ACKNOWLEDGEMENTS

We would like to express gratitude to Universidade Federal de Uberlândia for providing the computational resources used for the CFD simulation presented and for Programa de Pós-graduação em Engenharia Mecânica – FEMEC/UFU for fostering research activities. This study was financed in part by the Coordenação de Aperfeiçoamento de Pessoal de Nível Superior - Brasil (CAPES) - Finance Code 001.

10. REFERENCES

Baumgarten, C., 2006. *Mixture formation in internal combustion engines*. Springer Science & Business Media.

Duarte, C.A.R., Duarte, L.E.R., de Lima, B.S. and de Souza, F.J., 2020. "Performance of an optimized k- turbulence model for flows around bluff bodies". *Mechanics Research Communications*, p. 103518.

Fontes, D.H., Duarte, C.A.R. and de Souza, F.J., 2018a. "Numerical simulation of a water droplet splash: Effects of density interpolation schemes". *Mechanics Research Communications*, Vol. 90, pp. 18–25.

Fontes, D.H. *et al.*, 2018b. "Estudo numérico de jato líquido em escoamento cruzado usando uma abordagem híbrida".

Heywood, J.B., 1988. "Internal combustion engine fundamentals".

Ingle, R., Yadav, R., Punekar, H. and Cao, J., 2014. "Modeling of particle wall interaction and film transport using eulerian wall film model". In *ASME 2014 Gas Turbine India Conference*. American Society of Mechanical Engineers Digital Collection.

Kuhnke, D., 2004. *Spray/Wall-interaction Modelling by Dimensionless Data Analysis*. Ph.D. thesis, Darmstadt University of Technology, Darmstadt.

Morton, D., Rudman, M. and Jong-Leng, L., 2000. "An investigation of the flow regimes resulting from splashing drops". *Physics of Fluids*, Vol. 12, No. 4, pp. 747–763.

Ray, J., Lefantzi, S., Arunajatesan, S. and Dechant, L., 2014. "Tuning a rans ke model for jet-in-crossflow simulations." Technical report, Sandia National Lab.(SNL-CA), Livermore, CA (United States); Sandia National ....

Richards, K., Senecal, P.K. and Pomraning, E., 2016. "Converge v2. 3 manual". *Convergent Science, Inc., Madison, WI*.

Shedd, T. and Newell, T., 1997. "An automated optical liquid film thickness measurement method, air conditioning and refrigeration center, university of illinois, urbana-champaign, usa". Technical report, ACRC TR-134.

Shedd, T., Corn, M., Cohen, J., Arienti, M. and Soteriou, M., 2009. "Liquid film formation by an impinging jet in a high-velocity air stream". In *47th AIAA Aerospace Sciences Meeting including The New Horizons Forum and Aerospace Exposition*. p. 998.

Shim, Y.S., Choi, G.M. and Kim, D.J., 2008. "Numerical and experimental study on hollow-cone fuel spray of high-pressure swirl injector under high ambient pressure condition". *Journal of Mechanical Science and Technology*, Vol. 22, No. 2, pp. 320–329.

Sommerfeld, M., 2001. "Validation of a stochastic lagrangian modelling approach for inter-particle collisions in homogeneous isotropic turbulence". *International Journal of Multiphase Flow*, Vol. 27, No. 10, pp. 1829–1858.

Stanton, D.W. and Rutland, C.J., 1998. "Multi-dimensional modeling of thin liquid films and spray-wall interactions resulting from impinging sprays". *International Journal of Heat and Mass Transfer*, Vol. 41, No. 20, pp. 3037–3054.

Stevenin, C., Vallet, A., Tomas, S., Amielh, M. and Anselmet, F., 2016. "Eulerian atomization modeling of a pressure-atomized spray for sprinkler irrigation". *International Journal of Heat and Fluid Flow*, Vol. 57, pp. 142–149.

Versteeg, H.K. and Malalasekera, W., 2007. *An introduction to computational fluid dynamics: the finite volume method*. Pearson education.

White, F.M., 1962. *Mecânica dos fluidos*. McGraw Hill Brasil.

11. RESPONSIBILITY NOTICE

The authors are the only responsible for the printed material included in this paper.